ELECTRONIC SUPPLEMENTARY INFORMATION

SpectIR-fluidics: Completely customizable microfluidic cartridges for high sensitivity *in situ*

infrared spectroscopy with point-of-application studies on bacterial biofilms

Nan Jia,[a] Arthur Daignault-Bouchard,[b] Tianyang Deng,[a] Thomas G. Mayerhöfer,[c,d] André Bégin-Drolet[b] and Jesse Greener [a,e]

[a] Département de chimie, Faculté des sciences et de génie, Université Laval, Québec, QC G1V 0A6, Canada

[b] Département de génie mécanique, Faculté des sciences et de génie, Université Laval, Québec, QC G1V 0A6, Canada

[c] Leibniz Institute of Photonic Technology (IPHT), Jena, 07745, Albert-Einstein-Str. 9, Germany

[d] Institute of Physical Chemistry and Abbe Center of Photonics, Friedrich Schiller University, Jena, 07743, Helmholtzweg 4, Germany

[e] CHU de Québec, centre de recherche, Université Laval, Québec, QC G1L 3L5, Canada;

Index:

Section S1 – Materials and methods

Materials

Solutions of sodium phosphate dibasic (84486-300, Anachemia, Canada) and D-glucose (G8270-1KG, Sigma-Aldrich, Canada) were used as the test analytes. Amounts of 2.84 g of sodium phosphate dibasic (Na_2HPO_4) and 36.07 g of D-glucose ($C_6H_{12}O_6$) were each dissolved in 200 mL deionized water, resulting in separate solutions with respective concentrations of 0.1 M and 1.0 M. Different solution concentrations were obtained by serial dilution with DI water. The solutions were delivered to the spectIR-fluidic cartridge by syringe pumps (NE 1000X, New Era, USA) containing 30 mL syringes (BD-General Use-30mL, Fisher Scientific, Canada).

The microbial communities used in this study were isolated from the digestive tracts of *Tenebrio molitor* larvae (i.e., mealworms) and *Zophobas morio* larvae (i.e., superworms). In both cases, the insects were fed brown skin PVC prior to isolation. The insects were then dissected and the gut contents plated on Nutrient agar, and the colonies then pooled in nutrient broth (BD Difco Nutrient Broth, Fisher Scientific, Canada). The nutrient solution was prepared by dissolving 4 g of BD Difco Nutrient Broth powder in 500 mL of DI water and the nutrient solution was then autoclaved for sterilization. Prior to inoculation, the cartridge was first sterilized by flowing 75% ethanol for 20 minutes at a flow rate of 1.0 mL h^{-1}, followed by a flow of sterilized DI water at a flow rate of 5 mL h^{-1} for the same time. After that, a bacteria solution was injected into the SpectIR-fluidic cartridge, which had been incubated overnight prior to the experiment, and left static for 20 minutes before a sterile nutrient solution was admitted to feed the nascent biofilm.

SpectIR-fluidic cartridge materials

The microchannel layer used in these cartridges was fabricated using polydimethylsiloxane (PDMS) mixed with a cross-linking agent (Sylgard184, Dow Corning, Canada) at a ratio of 10:1 that was cast against a mould. All moulds were fabricated by photolithography using a laminate photoresist with 50 µm thickness (SF4000, Mungolux, Germany) adhered to glass. The channel geometries were designed by computer-aided design software (AutoCAD, Autodesk, USA). The surface metrology of the embedded ATR sensing layer was measured with an optical profilometer (ContourX-200, Bruker, USA). Multi-ridge ATR crystals (Basic Universal, IRUBIS GmbH, Germany) were used without further modifications. The ATR crystal dimensions were 11 mm by 9 mm, but these included a 1 mm border around its edge that was not coupled to the ridges or its bottom side. Therefore, the sensing region measured only 9 mm by 7 mm.

Fourier transform infrared spectroscopy

To demonstrate the generality of the technique, measurements were collected on either a portable FTIR spectrometer (Alpha II, Bruker Ltd. Canada) with a room-temperature DLaTGS

detector and computer control software (OPUS, Bruker, USA) or on a research-grade spectrometer (Nicolet iS50, Thermo Fisher Scientific, USA) with a nitrogen-cooled MCT detector, computer control software (OMNIC, Thermo Fisher Scientific, USA), and an anti-vibration table. The beam splitters in both spectrometers were KBr. In all cases, a purge gas generator was used to limit atmospheric interference. The portable FTIR system was used for biological experiments using bacterial biofilms to demonstrate applications that may require that measurements which are done at point of source or within biosafety enclosures. Unless otherwise noted, all other experiments were run on the iS50 research-grade spectrometer with 32 co-additions, a scan velocity of 1.90 cm s^{-1} (15 kHz) and a spectral resolution of 4 cm^{-1} unless otherwise stated. In some cases, spectra were collected using a portable spectrometer with 64 co-additions, a scan velocity of 0.96 cm s^{-1} (7.5 kHz), and a spectral resolution of 8 cm^{-1}. The spectIR-fluidic cartridges were interfaced with a customized accessory for spectroscopy and chemical mapping in microfluidic channels (referred to herein as a spectIR-fluidic interface and mapping accessory)[18] for spatially selective measurements.

Data analysis

Spectral processing and analysis were carried out using open-source software (Quasar, Orange, Slovenia).[20] A linear baseline correction was first applied between 1400 cm^{-1} and 800 cm^{-1}, which zeroed measurements of the analyte absorbance band heights. For D-glucose ($C_6H_{12}O_6$), the characteristic COC backbone vibration was observed at 1100 cm^{-1}.[21] For the prepared 0.1 mol L^{-1} solution of sodium phosphate dibasic (Na_2HPO_4), which partitions into different protonation states depending on pH, two characteristic absorbance peaks were analyzed in this work, corresponding to $H_2PO_4^-$ (1072 cm^{-1}) and HPO_4^{2-} (990 cm^{-1}).[22] Either peak heights or peak areas were used for absorbance quantification. For example, a linear regression algorithm was used to obtain calibration curves of absorbance versus analyte concentration. From the resulting equation, we calculated the limits of detection LOD (M) and limits of quantification LOQ (M) based on the concentrations that produced peak heights equal to 3 and 10 times the noise floor, respectively. Noise was quantified from the root mean square error using noise spectra in the same spectral window corresponding to the absorption band of interest.

Computational fluid dynamics simulations

Computational fluid dynamics simulations (COMSOL Multiphysics V5.4, Stockholm, Sweden) were used to determine the flow velocities and concentration profiles under steady-state conditions. This was achieved with laminar flow and transport of diluted species modules and

a   Navier-slip boundary condition at the channel walls. Diffusion coefficients of $D_{HPO_4^{2-}}$ =

0.69×10^{-9} m^2 s^{-1} and D_{H+} = 9.31×10^{-9} m^2 s^{-1} were used for phosphate and hydrogen ions, respectively. Liquids were treated as incompressible Newtonian fluids under isothermal laminar flow conditions. A triangular mesh was built with the aid of an adaptive meshing algorithm, resulting in a total of 1101086 elements covering the entirety of the model area

(total of 51.65 mm^2). A PARDISO numerical solver was used to solve the system, and the relative tolerance for the convergence criteria value was 0.001.

Section S2 – ATR sensing layer jig

Figure S1 shows renderings of the computer aided design and an image of the jig that was used to fabricate the ATR sensing layer.
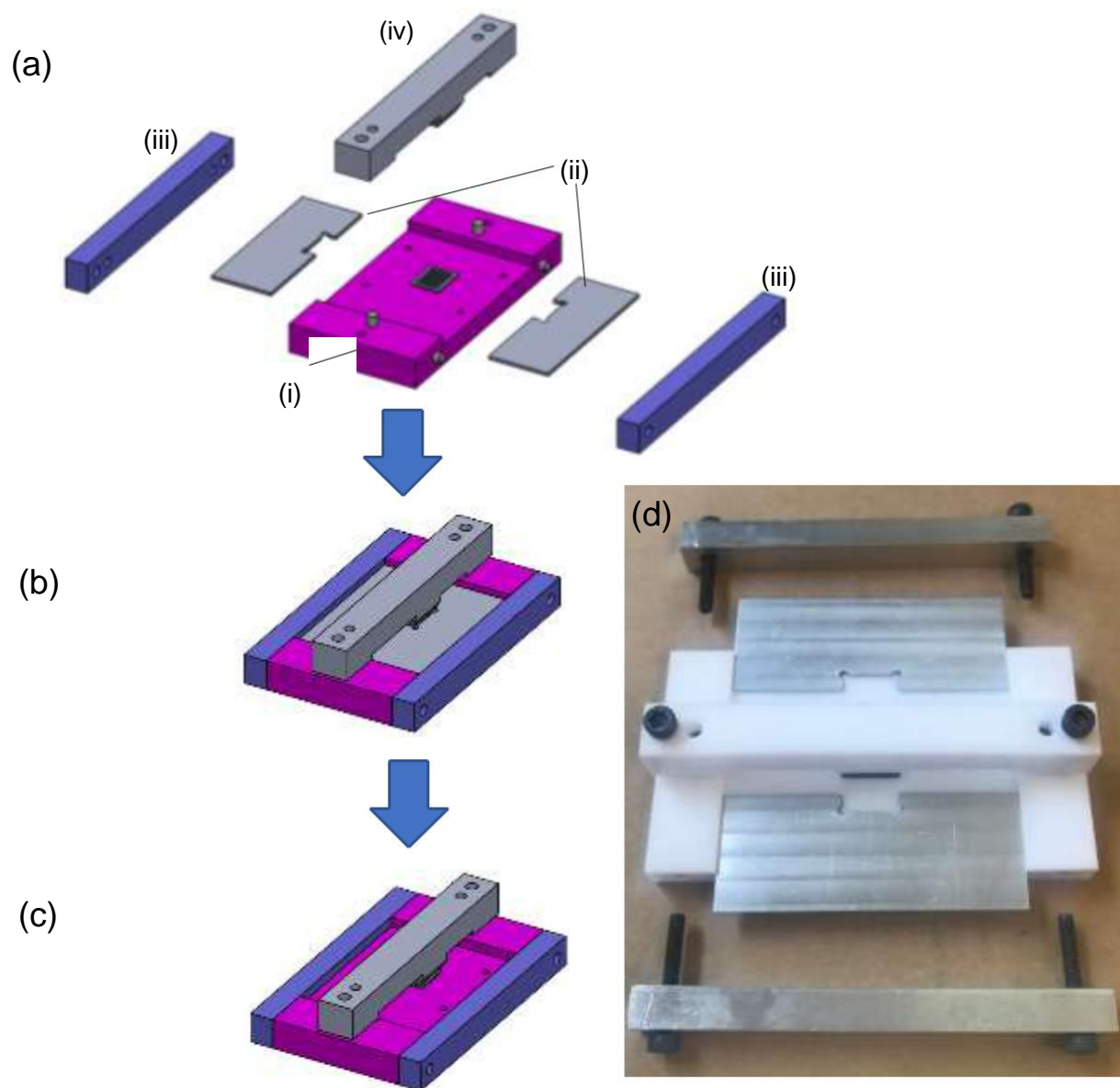

Figure S1. ATR alignment jig for fabrication of the ATR sensing layer. Computer aided design renderings of: (a) exploded view showing (i) jig baseplate (pink) with ATR crystal placed sensing side down (grey), (ii) guiding plates, (iii) connecting sidebars and (iv) ATR immobilizing arm and Teflon plug with tapered edges. CAD of (b) the assembled view of jig

with ATR guiding plates installed and (c) with the plates removed, in advance of pouring the PDMS. The glass-supported polyethylene thin film is not shown. (d) An image of the machined jig components.

Section S3 – Topography of the PDMS/ATR interface

We used an optical profiler to inspect the region around the Si ATR crystal to determine the topography in the transition zone from the ATR sensing surface to the surrounding PDMS material (Figure S2a). As shown by Figure S2b, there is a small reduction in the channel floor around the ATR crystal, averaging 4.8 µm. The PDMS floor recovers to the baseline channel elevation about 0.8 mm away from the Si crystal. Therefore, this reduction in height is very shallow, with a maximum aspect ratio (height to width) of 6×10^{-3}. We calculated that the trough around the crystal represents a dead space of approximately 80 nL. It should be noted that this did not cause any channel cross-talk, likely because the low aspect ratio of the recessed portion is accessible for bonding with the (flexible) PDMS channel layer.
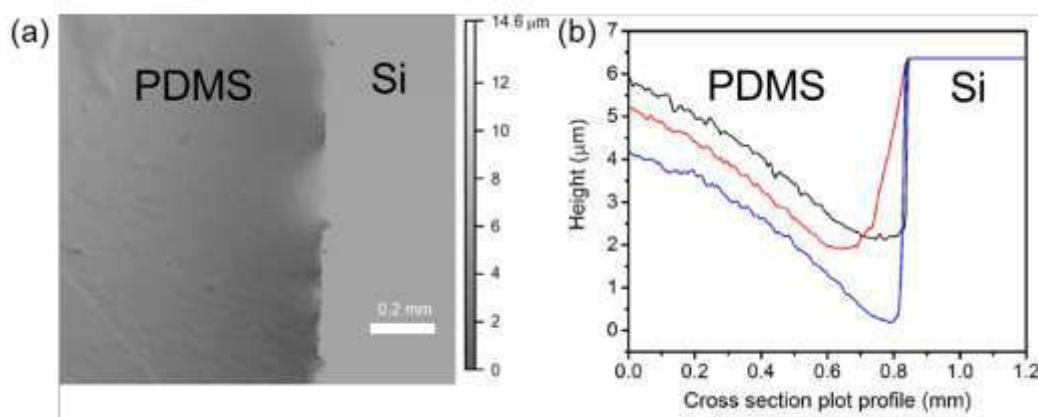

Figure S2. (a) Profiler images of the crystal part at the junction between the PDMS and Si ATR crystal and (b) three linear profiles obtained from horizontal traces across (a) from left (PDMS side) to right (Si ATR side). Note that in (b), the x- and y-axes are given in different units.

Section S4 – Effect of ATR crystal orientation on spectral line shape

Spectra of water obtained from two spectIR-fluidic devices with perpendicular and parallel orientations (Figure S3a). For the parallel oriented ridges there is only one inner angle of incidence (Figure S3b) yielding typical "symmetric" lineshapes, similar to those seen previously in the literature.[1] Perpendicular oriented ridges (Figure S3c), results in complicated non-symmetrical lineshapes because the angles of incidence relative to the down-and up-stream ridge edge are different. One is given by ϴ - AOI (at the upstream side of the ridge), leading to an inner AOI of $\gamma_{1,i} = 30.7°$ which is well above the critical angle, while the other is

Ɵ + AOI (at the downstream side of the ridge), leading to $\gamma_{2,i}$ = 21.1° and conventional reflection, which means that part of the light is transmitted. Thus, the spectrum consists of a mixture of two parts: One part is strongly influenced by the refractive index function, while for the other (ATR spectrum), the penetration depth of the light into the sample is smaller, leading to smaller absorbance values according to Beer's approximation.[2,3]

Overall, the perpendicular orientation relative to the light path offers the ability to obtain quantitative concentration profiles, in contrast to the parallel orientation, because, although the band shapes are changed, their areas are still directly proportional to the molar concentrations as discussed in the ESI (Section S5). Additionally, as the x-scan direction of the ridges in the parallel orientation results in oscillations in the absorbance value, whereas it is continuous for the perpendicular ridges. Therefore, the latter holds the potential for chemical mapping.
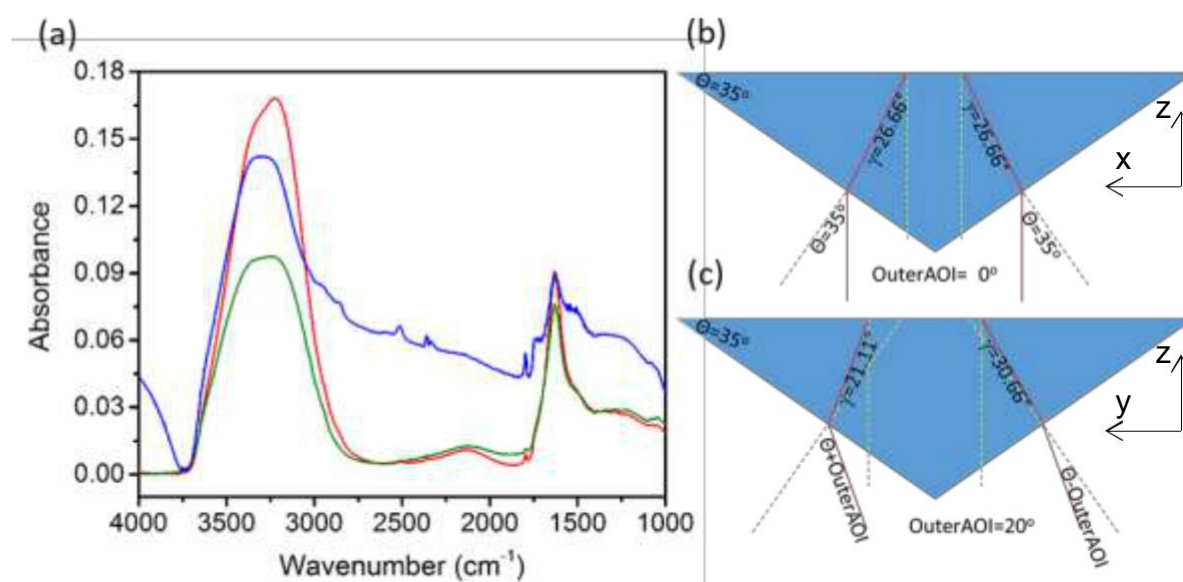

Figure S3. Water absorbance spectra. Spectra were obtained in the parallel ridge orrientation with aperture illuminating the middle ridge (red) at maximum intensity (x=-0.1 mm) and the interstiatial position beside that ridge (green) and in the perpendicular orientation (blue) near the middle portion of the channel. Illustration the influence ATR ridge orientation on outer and inner angles of incidences for parallel (b) and perpendicular (c) orientations, respectively. Note the direction of an x-scan is horizontal for (b) and perpendicular to the page for (c).

Section S5 – Representative spectra from dynamic experiments on a compact spectrometer

To obtain rapid spectral acquisition for experiments with dynamic solution profiles, we acquired only two spectral co-additions. Figure S4 shows the resulting absorbance spectra for Na_2HPO_4 and H_2O using a H_2O single-beam spectrum as the background. Though the noise was high, the characteristic HPO_4^{2-} band was easily identified.
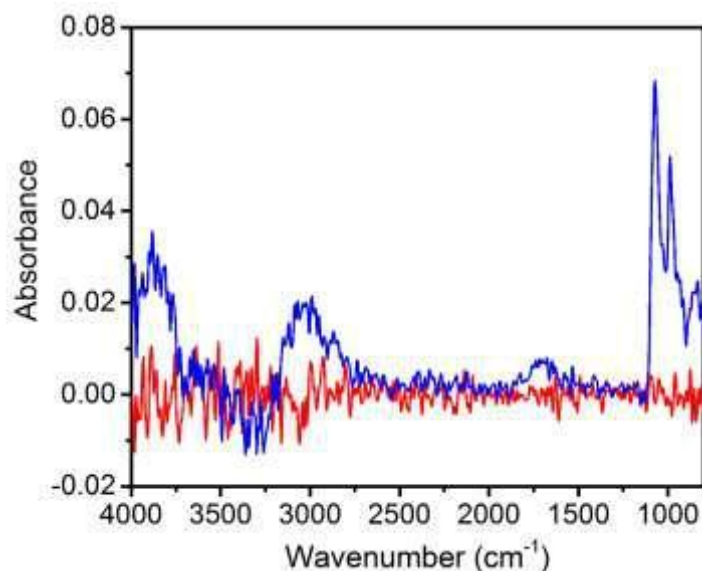

Figure S4. Representative spectra obtained from the dynamic concentration experiment using two scans at 8 cm^{-1} on a compact spectrometer. Na_2HPO_4 (0.1 M) is shown in blue, and the noise spectrum obtained using water as the background and as the sample is shown in red.

Section S6 – Supplementary dynamic flow experiments

We demonstrated the generality of the technique shown in the main paper by oscillating between water and DMF. Both solvent spectra in Figure S5a are shown relative to an air background to show the peaks for each solvent, as opposed to Figure 2c in the main paper in which water was used as a background. In Figure S5a, the water bands are visible, which enables a direct evaluation of any potential residual solvent from the previous flow pulse. Figure S5b shows the integrated band intensity as a function of time. The peak areas always returned to a zero value when flowing the other solvent, indicating that no residual solvent remained in the channel when one solvent was flowing.
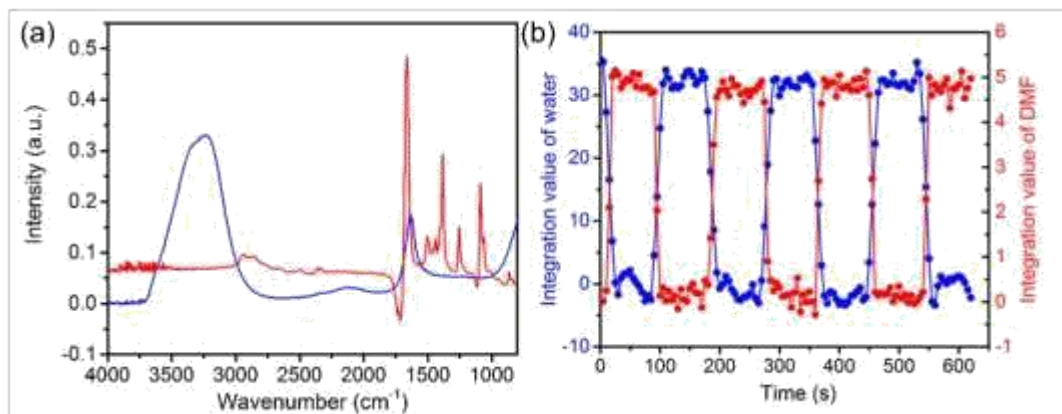
Figure S5. (a) Individual spectra of water (blue) and DMF (red) with the unique peaks used for liquid identification highlighted. (b) Result from alternating flow of water and DMF (10 mL h^{-1}).

Section S7 – Supplementary assays (water and DMF)

We used an air background obtained separately from each channel to observe the water and DMF spectra, similar to Section S6. This enabled a more direct route to validation of the functionality of the device without cross-contamination. Figure S6 shows the individual spectra from each channel. No water bands at 3400 cm^{-1} are observed in the DMF spectra. Similarly, no DMF-specific bands (e.g., 1089 or 1385 cm^{-1}) are observed in the water channels. This proves the measurement independence of each channel and expands the range of compatible solvents with the technique. Finally, we flowed water in one channel while maintaining dry conditions in the neighbouring channels to definitively test for potential leaking between channels. No absorbance bands were observed in neighbouring channels after 1 hour of flow at 5 mL h^{-1}. This result validated the strict inter-channel isolation of the device.
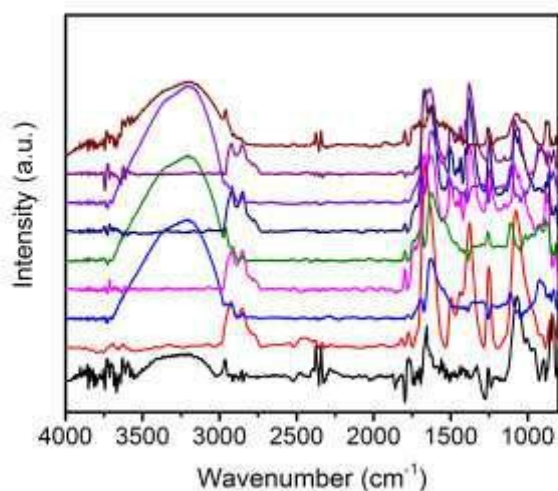
Figure S6. Spectra obtained from each channel of the nine-channel assay device with alternating flow streams of water and DMF.

Section S8 – Biofilm growth curves

A continuous measurement was conducted on the growing biofilm (see main paper Figure 7a). Each measurement resulted in a spectrum with peaks (see table S1) intensities that changed in time, which were measured to obtain an absorbance versus time curve (Figure S7). After a short lag-phase (0-2 hours) a rapid growth phase is visible, during which all peaks increased at a nearly exponential rate. This was followed by a stable period (stationary phase) until 32 hours, when an event removed much of the detected molecular signature. We attribute the loss of spectral intensity to a sloughing event, whereby shear forces increased due to the excluded free space resulting from the increasing biofilm volume. It is interesting to note that the signal arising from phosphorylated proteins at 1083 and 1232 cm^{-1} were not affected by this event, confirming a role in cell/surface adhesion.[4]
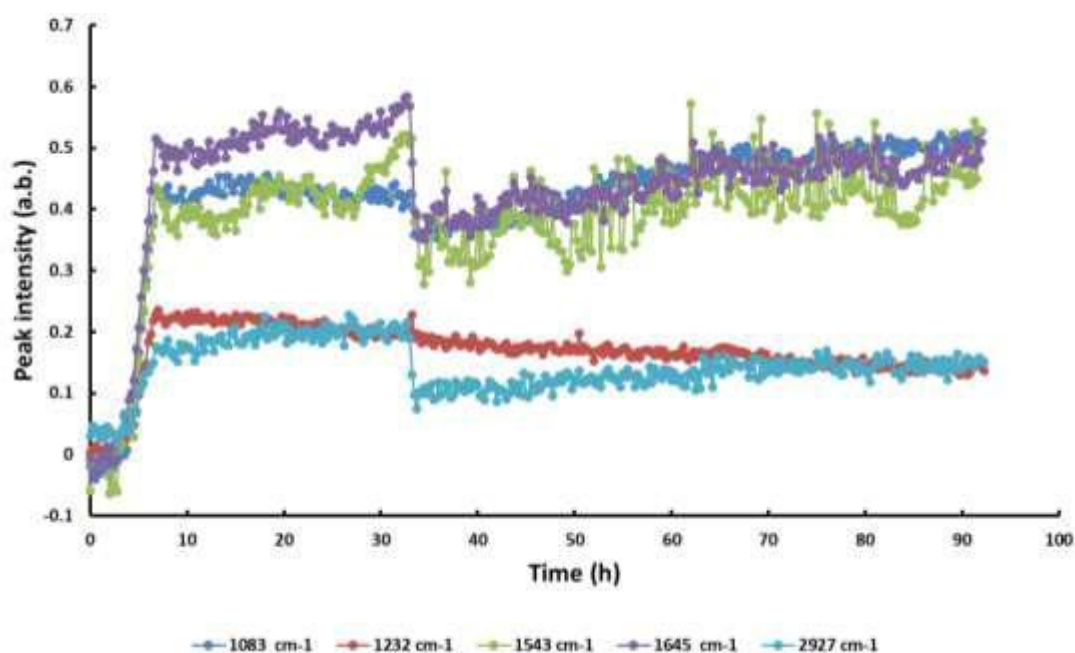

Figure S7. Peak intensity vs time of different peaks.

Table S1. Band assignments for typical bacterial biofilms.[5]

Wavenumber	1083 cm^{-1}	1232 cm^{-1}	1543 cm^{-1}	1645 cm^{-1}	2927 cm^{-1}
Group	PO_2^-	PO_2^-	Amide II	Amide I	CH_2
Mode	Symmetric stretch	Asymmetric stretch	Composite C=O, C-N, HOH distorsion	Composite N-H, C-N, HOH distortion	asymmetric stretch
Source	Phosphorylated proteins	Phosphorylated proteins	Proteins, peptides	Proteins, peptides	Lipids

Section S9 – Supplementary references

1. M. Joly, T. Deng, T. A. Morhart, G. Wells, S. Achenbach, A. Bégin-Drolet and J. Greener. *Anal. Chem*., 2021, **93**, 14076-14087

2. G. Falcon-Millan, M.P. Gonzalez-Muñoz, A. Durand, J. A. Reyes-Aguiler, T. A. Razo-Lazcano and M. Avila-Rodriguez. *J. Mol. Liq.*, 2017, **241**, 967-973.

3. J.-J. Max and Chapados. *J. Chem. Phys*., 2009, **131**, 184505.

4. A. Rajah, C. G. Boudreau, A. Ilie, T-L. Wee, K. Tang, A. Z. Borisov, J. Orlowski and C. M. Brown. *Sci. Rep*., 2019, **9**, 11430.

5. B. Gieroba, M. Krysa, K. Wojtowicz, A. Wiater, M. Pleszczyńska, M. Tomczyk and A. Sroka-Bartnicka. *Int. J. Mol. Sci*., 2020, **21**, 3811.